Nonlinear multi-frequency transmitter for seafloor characterization

Lucilla Di Marcoberardino[1,2,3,4], Jacques Marchal[1,2] and Pierre Cervenka[2,1]

[1] UPMC Univ Paris 06, UMR 7190, Institut Jean le Rond d'Alembert, F-78210 Saint-Cyr-l'Ecole, France
[2] CNRS, UMR 7190, Institut Jean le Rond d'Alembert, F-78210 Saint-Cyr-l'Ecole, France
[3] CNR, Istituto di Acustica 'O.M. Corbino', I-00133 Roma, Italy
[4] SAPIENZA Università di Roma, Facoltà di Ingegneria, I-00184 Roma, Italy

Summary

To gather with a single surveying tool the backscatter frequency response of the seafloor would be a large asset to characterize the nature of the bottom. One proposes to take advantage of the saturation effect occurring with a high powered source: numerous harmonic waves are created by non linear interactions along the propagation. The feasibility of a multi-frequency source that is adapted to seafloor characterization is investigated. In a preliminary approach, a pseudo-1D model is used to estimate the on-axis levels of the first multiple frequencies. Experimental measurements performed with two typical geometries of transducers are compared with simulations.

PACS no. 43.25.Cb, 43.25.Jh, 43.25.Lj, 43.30.Lz, 43.30.Yj.

1. Introduction

In the underwater acoustic domain, there is a large interest for techniques able to achieve seafloor characterization. Typical applications are related to geology (local basin monitoring surveys), industry (installation and monitoring of underwater deployed structures), and environment (coastal protection and management). Classical acoustic surveying tools are sidescan sonars and multibeam echo-sounders which provide images of the backscattered acoustic intensity, and maps of the relief. Each individual system does not offer frequency or spatial diversities: the frequency bandwidth is narrow; under usual conditions, each patch of the seafloor is seen from a single angle of view. However, it is known that the frequency and angular backscatter responses would be very helpful to determine the nature of the seafloor, and large efforts are deployed to take advantage of such diversities. For example, enabling multiple angles of view has been investigated with a forward looking geometry [1]. Another investigation consisted of surveying the same seafloor areas [2] with several systems offering various space-time characteristics. A typical illustration of the potential interest of the multi-frequency approach is given by an experiment on the capability to detect sunken oil slicks [3] with several surveying tools: high frequencies reveal flat superficial spots through no bascattered energy; low frequencies enable to see the underlying substrate; the combination of both information allows to infer the presence of thin oil slicks.

When running concurrent systems, a major challenge is to correlate in a consistent way data obtained in different conditions. We propose to investigate a new concept based on a transmitter that generates simultaneously several harmonic frequencies. The source is unique in time and space so that the multi-frequency responses are inherently perfectly matched. The acoustic beams would be generated through the harmonic components of a shock wave

radiated by an antenna driven at a high level. Note that depending on the implementation, the multiplicity of points of view can be also included.

Using the second harmonic that is generated by the nonlinearity of the propagation is a well known technique in the medical domain to improve the resolution of the echographic acoustical images [4, 5, 6, 7, 8]. In the underwater acoustic domain, the nonlinearity of the propagation is always perceived as a drawback, but for the parametric antennas application [9], because it leads to losses of efficiency in transmitting antennas [10]. When increasing the transmitted power, part of the acoustical energy is transferred along the propagation to higher harmonic components. It leads to a saturation effect on the fundamental frequency which limits the source level that can be reached [11]. At the present time, there is no significant study on the harmonic fields generated by nonlinear propagation within the context of the devised application in underwater acoustics. Our present concern is the feasibility of such a multi-frequency tool with the suitable characteristics needed to handle surveying tasks. The main challenge is to obtain sufficient source levels, while keeping large enough angular apertures for the generated harmonic beams.

We present here a preliminary study in which a simplistic theoretical model (Section II) is faced with experimental measurements (Section III). The developed model gives only on-axis level estimates. It is based on the generalized Burgers equation [12] whose numerical implementation is straightforward. The experimental investigation is made with two transducers whose beam patterns are very different: a directive disk and an elongated rectangle. Comparisons between measurements and estimations are presented in Section IV.

2. Pseudo-1D model

2.1. Theory

Most of the existing codes that have been developed to compute finite-amplitude acoustic fields of progressive waves are based on the KZK equation [13, 14, 15 ,16, 17], which is only adapted for directive beam patterns because of the paraxial approximation. There is a current effort to develop tools that enable to model wide beams [18]. Within the scope of a preliminary approach, we made an attempt to develop a very simple pseudo-1D model for estimating on-axis levels only. It is still based on the generalized Burgers equation, including the effect of the diffraction by means of a single parameter [19]. We recall in the following the various elements that build the model equation when taking into account the attenuation, diffraction and non linear effects.

The 3-D quadratic nonlinear equation for fluids reads in terms of the acoustic potential $\Phi(\mathbf{r},t)$ [9, 19]:

$$\Delta\Phi - c_0^{-2}\Phi_{tt} = 2c_0^{-1}\mathcal{L}(\Phi_t) + c_0^{-2}\frac{\partial}{\partial t}\left[(\nabla\Phi)^2 + (\beta-1)c_0^{-2}(\Phi_t)^2\right] \tag{1}$$

(derivatives are denoted $\partial\Phi/\partial t = \Phi_t$). c_0 is the small-signal sound speed and β the coefficient of nonlinearity ($\beta = 3.5$ in fresh water). $\mathcal{L}(\Phi_t)$ is a linear operator which describes different phenomena related to attenuation. In the Kuznetsov equation [20], this operator takes into account the only thermovicous attenuation:

$$\mathcal{L}(*) = -\frac{b}{2\rho_0 c_0^3}\frac{\partial^2 *}{\partial t^2}. \tag{2}$$

where b is the viscosity coefficient and ρ_0 the density of the medium. In the sea water [21], the relaxation must be included so that the operator $\mathcal{L}(*)$ becomes:

$$\mathcal{L}(*) = -\frac{b}{2\rho_0 c_0^3}\frac{\partial^2 *}{\partial t^2} - \sum_i \frac{\Delta c_i}{c_0^2}\int_{-\infty}^{t}\frac{\partial^2 *}{\partial t'^2}\exp\left(-\frac{t-t'}{\tau_i}\right)\mathrm{d}t' \quad (i = 1,2). \tag{3}$$

The relaxation times $\tau_{1,2}$ and the velocity increase $\Delta c_{1,2}$ characterize the two relaxation processes. However from a pratical point of view, it is more convenient to handle the attenuation as a function of the frequency f by using the attenuation coefficient $\alpha(f)$:

$$\mathcal{L}\left(e^{j2\pi ft}\right) = \alpha(f)e^{j2\pi ft}. \tag{4}$$

In the sea water, the Francois-Garisson model [22] is commonly admitted.

In the pseudo-1D model, the wave energy is assumed to be collimated in the near field (plane wave), and uniformly distributed over a cone in the far field (spherical spreading). The angle θ_a of the cone corresponds to the -3dB beam width. As a consequence, the transition between these two zones occurs at the Fraunhofer (or Rayleigh) distance $L_F=a^2/\lambda_0$, where a denotes the characteristic lateral dimension of the source and λ_0 is the wavelength at the fundamental frequency (note that $2\theta_a \equiv a/\lambda_0$). With a rectangular projector (Figure 1), two transitions distances L_{Fa} and L_{Fb} must be introduced, the zone lying in between corresponding to a cylindrical propagation [23].

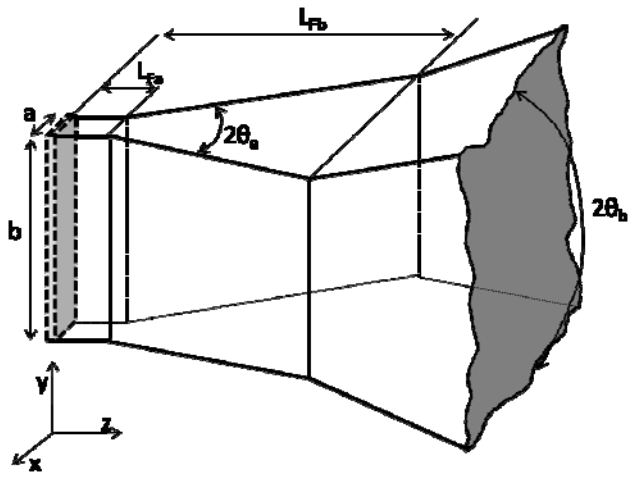

Figure 1. Scheme of the energy distribution in the pseudo-1D model.

To take into account the diverging character of the different progressive waves, the Laplacian operator is made explicit with:

$$\Delta\Phi = \Phi_{rr} + \frac{2m}{r}\Phi_r, \tag{5}$$

where $m = 0, 1/2, 1$, respectively for plane, cylindrical and spherical waves. The main hypothesis in this model is that the acoustic field is homogeneous within each defined zone, so that the potential depends only on $r = |\mathbf{r}|$ and t. Because it is a pseudo-1D model, one imposes $r = z$ in the plane wave zone.

Introducing the retarded time $\theta = t - r/c_0$, the potential undergoes the following transform:

$$\varphi(r,\theta)=\Phi(r,t)\,. \tag{6}$$

The spatial variation of the field $\varphi(r,\theta)$ over wavelength-like distances at a fixed time is much smaller than the time variation at a fixed place $\left(|\varphi_r|\ll|\varphi_\theta|\right)$, so that:

$$\Phi_r=\varphi_r-c_0^{-1}\varphi_\theta\approx-c_0^{-1}\varphi_\theta\,. \tag{7}$$

Using (6)(7) in (1) yields:

$$\varphi_{r\theta}+\frac{m}{r}\varphi_\theta=-\mathcal{L}(\varphi_\theta)-\frac{\beta}{2c_0^3}\frac{\partial(\varphi_\theta)^2}{\partial\theta}\,. \tag{8}$$

Integrating with time gives:

$$\varphi_r=-\mathcal{L}(\varphi)-\frac{m}{r}\varphi-\frac{\beta}{2c_0^3}(\varphi_\theta)^2\,. \tag{9}$$

The observable parameters are the acoustic velocity **v** and pressure *p* which are related to the potential through

$$\begin{cases}\mathbf{v}=\mathbf{grad}(\Phi)\\ P=-\rho_0\Phi_t-\dfrac{\rho_0}{2}\left[(\nabla\Phi)^2-c_0^{-2}(\Phi_t)^2\right]\end{cases} \tag{10}$$

In the retarded time referential, there is with (7) the approximate relations

$$\begin{cases}v_r\approx-c_0^{-1}\varphi_\theta\\ P\approx-\rho_0\varphi_\theta\end{cases} \tag{11}$$

Consequently, (8) reads in terms of pressure:

$$P_r=-\mathcal{L}(P)-\frac{m}{r}P+\frac{\beta}{2\rho_0c_0^3}\frac{\partial(P)^2}{\partial\theta}\,. \tag{12}$$

This equation is the generalized Burgers equation that models diverging waves in the case of attenuating and relaxing media [12, 19]. Denoting v_0 the velocity normal to the surface of the projector, (12) can be written in the dimensionless form with $p=P/\rho_0c_0v_0$:

$$\frac{\partial p}{\partial r}=-\frac{m}{r}p-\frac{1}{L_\alpha}\mathcal{L}'(p)+\frac{1}{L_s}p\frac{\partial p}{\partial\tau}\quad\text{with}\quad m=\begin{cases}0\ \text{ if }\ r<L_F\\ 1\ \text{ if }\ r\geq L_F\end{cases} \tag{13}$$

Equation 12 outlines the influence of each of the phenomena that dictate the pseudo-1D propagation through the following characteristic distances: $L_\alpha = 1/\alpha(f_0)$ is the attenuation distance; $L_s=c_0^2/(v_0\beta\omega_0)$ is the shock formation distance; $\tau=2\pi f_0t$ is the dimensionless time; $\mathcal{L}'=\mathcal{L}/\alpha_0$ is the dimensionless attenuation propagator which simplifies into $\mathcal{L}'=\partial^2/\partial\tau^2$ with pure fresh water. The relative magnitudes of the lengths L_s, L_F and L_α reveal the relative influence of each effect during the propagation. It is therefore convenient to introduce the ratios coined as the Khokhlov's number $\mathrm{K}=L_F/L_s$, and the Goldberg's number $\Gamma=L_\alpha/L_s$. In order to observe the definite influence of the non linear distortion, L_s must be smaller than, or at the same order of magnitude as both L_F and L_α, i.e., $\mathrm{K}\leq 1$ and $\Gamma\leq 1$.

2.2. Numerical implementation

A well known modus operandi is the fractional-step procedure performed along the main propagation direction r [24]. At each step Δr, each phenomenon is processed separately. If the step is "small enough", the evolution of the waveform caused by each effect is so small that the result is independent of the process order [16]. The second order accuracy can be reached by using for instance the Strang splitting scheme [25]. Hence, the step value is derived from a reference length that is defined as the smallest of L_α, L_F and L_s.

Another point to be considered is the choice of the computational domain in the numerical implementation, i.e., frequency [13] or time [14, 26]. The results presented next are obtained with a hybrid method [27][28][29]: the nonlinearity is addressed in the time domain, whereas geometrical spreading and absorption are processed in the frequency domain. Note that the two latter contributions are handled with exact solutions, i.e.,

$$\frac{\partial p}{\partial r}+\frac{m}{r}p=0 \quad \rightarrow \quad p/r^m=\text{const.} \tag{14}$$

$$\frac{\partial p}{\partial r}=-\frac{1}{L_\alpha}\mathcal{L}'(p) \;\rightarrow\; p(f)e^{+\alpha(f)r}=\text{const.} \tag{15}$$

The nonlinear contribution is evaluated by using a development of the Poisson's implicit solution:

$$\frac{\partial p}{\partial r}=\frac{1}{L_s}p\frac{\partial p}{\partial \tau} \quad \rightarrow \quad p(r+\Delta r,\tau)\approx p\left(r,\tau+p\frac{\Delta r}{L_s}\right). \tag{16}$$

The solution is obtained in this scheme by interpolating the sound pressure signal at each step with a distorted time. In order to avoid multi-valued solutions, it is sufficient to take provision that the maximum time shift in (16) remains smaller than the numerical time sampling $\Delta\tau$, i.e.,

$$\max(|p|)\frac{\Delta r}{L_s}\le\Delta\tau\,. \tag{17}$$

This condition is always verified if $\Delta r \le L_s/N$, with N as the number of samples per period. Note that a more efficient process would implement a variable step Δr that increases while the pressure decreases, e.g., the evolution being dictated by (17).

3. Experiments

Two projectors have been built to test the multi-frequency propagation feasibility: a circular and a rectangular transducer working in piston mode (Table I). The disk produces a rather directive beam (~5°); the rectangle features a rather wide aperture in one of the two principal planes (~50°), hence being closer to the classical configuration used with side scan sonars.

Table I. Characteristic values of the sources

Geometry	**Disk**	**Rectangle**
Size	∅ 18 cm	1.6 cm × 26 cm
f_0	100 kHz	
λ	1.50 cm	
Aperture (–3dB)	4.8°	47° × 3°
L_F	1.7 m	1.7 cm and 4.5 m
L_α	235 m	
Sv @ 100 kHz	173 dB/V	160 dB/V

The size of the tank is 12 m × 6 m × 3 m. It contains fresh water. A hydrophone (Reson TC4034, 1 Hz – 500 kHz) is deployed from a mobile deck. An automated translation capability enables to scan a 3 m × 2 m surface with the hydrophone.

The sound speed is evaluated with the Lovett model [30]. During the experiments, it ranges between 1480 m/s (T = 12.3 °C spring time – circular projector measurements) and 1420 m/s (T = 3.7 °C winter time –rectangular projector measurements).

The power is provided by a custom E/D class amplifier that delivers up to 20 kW electric. The signal output by the amplifier is square shaped. Consequently, its spectral content is a combination of odd harmonics. The transducer does not filter all these components, especially the 3rd harmonic. If the power signal is applied to the antenna without any filtering, it raises an issue about the interference between the acoustic contribution that is directly transmitted, and the field that is created at the same frequency because of the non linear propagation. Preliminary tests showed that this interference is actually destructive. The filter that is inserted in the matching circuit reject all the harmonics down to more than –30dB. On the other hand, the applied voltage level is very conservative with respect to the limits of the PZT material, so that there is no nonlinearity in the transduction process. But for a possible cavitation phenomenon, the harmonic content of the acoustic source can be thus assumed to be negligible compared to the equivalent source level created at these frequencies by the non linearity of the propagation. In addition, the source level at the fundamental frequency can be directly estimated from the voltage feeding the antenna and the sensitivity of the transducer (established with low transmitting levels - see Sv Table I). Table II displays the acoustic levels obtained as a function of the nominal electric power delivered by the amplifier (the global electric-acoustic efficiency of the transmitter is in the range 30 % – 60 %).

Comparing the characteristic distances in Tables I and II, it appears that L_α is always much larger than L_s and L_F, so that the attenuation is never the dominant effect. On the other hand, it can be seen that diffraction and non linearity are competing effects

Table II. Source levels (dB re 1 μPa rms) and shock distance in function of the applied power.

	Circular projector		
P_e	P_0	P @ 1 m	L_s
1.2 kW	216 dB	221 dB	16.2 m
5 kW	222 dB	227 dB	8.4 m
20 kW	228 dB	233 dB	4.3 m

	Rectangular projector		
P_e	P_0	P @ 1 m	L_s
1.2 kW	225 dB	214 dB	6.0 m
5 kW	231 dB	219 dB	3.0 m
20 kW	236 dB	225 dB	1.6 m

The active surface of the transmitters is driven with a uniform normal velocity v_0. In Table II, the equivalent pressure is defined as $P_0 = \rho_0 c_0 v_0$. This value gives an indication that cavitation may occur if $P_0 > 220$ dB (1 bar). The actual threshold of this phenomenon depends on different parameters, such as frequency, pulse length and static pressure. In the experiments, the measurements are repeated for several pings in order to check the stability of the results. Fluctuations in the recorded levels are observed (at 6-m distance) beyond a certain threshold in the applied electrical power (Figure 2): 11 kW for the circular source and 2.8 kW for the rectangular one. Although there is no clear evidence, cavitation is the most likely cause. Consequently, the analysis presented hereafter concerns only measurements obtained below these limits. There are also variations in the 4^{th} harmonic levels observed at low transmit power: this is simply caused by the limited dynamic range of the acquisition system combined with the noise level.

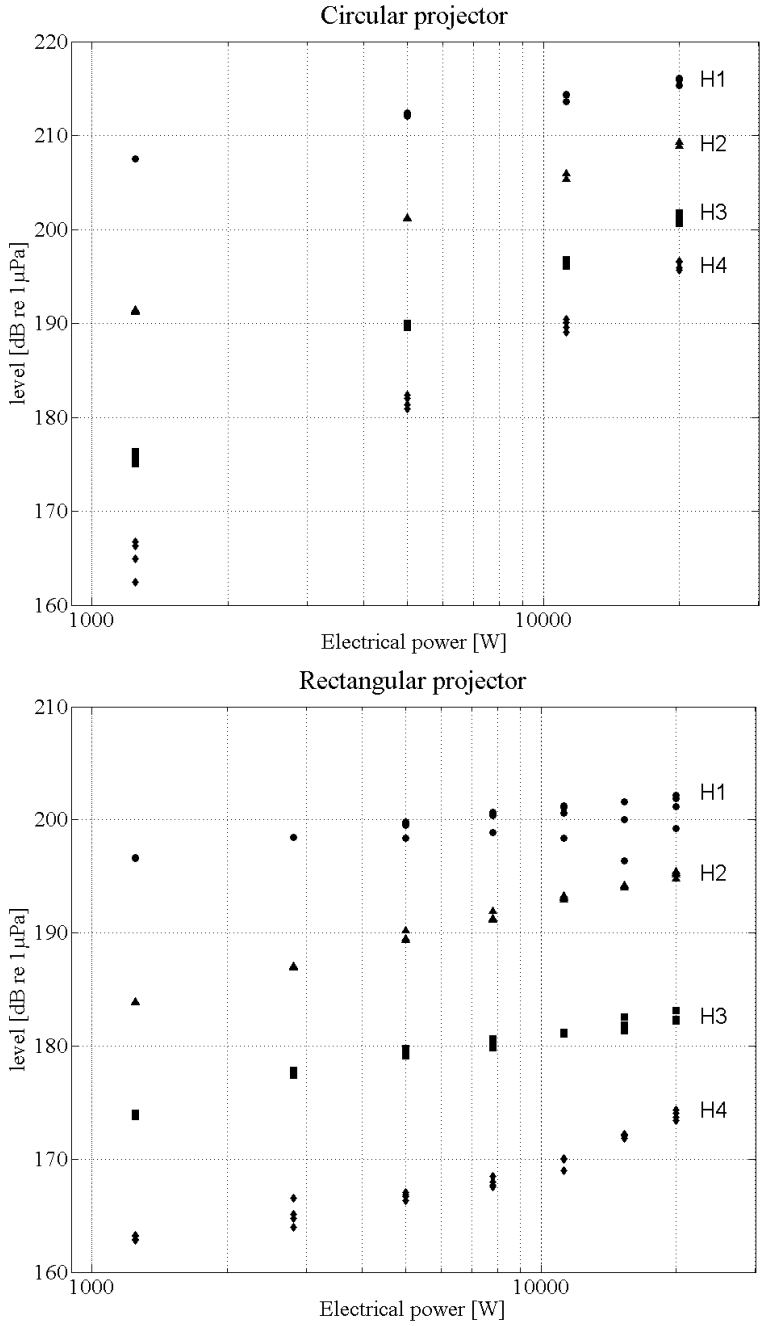

Figure 2. Harmonic levels versus electrical power, measured at $z = 6$ m.
Top: circular projector. Bottom: rectangular projector.

4. Results

4.1. On-axis levels

The on-axis levels are displayed straightforwardly as measured at several distances (i.e., no conversion at the equivalent source level at 1 m distance). Experimental results are superimposed with the estimations obtained with (13), which are computed with the input values given in Tables I and II. Despite the simplistic model for taking into account the geometrical spreading, there is a good agreement with the circular antenna (Figure 3). As

previously observed, the dynamic range is too large between H1 and H4, at low power input, to give accurate measurements of the H4 level with the acquisition system in use.

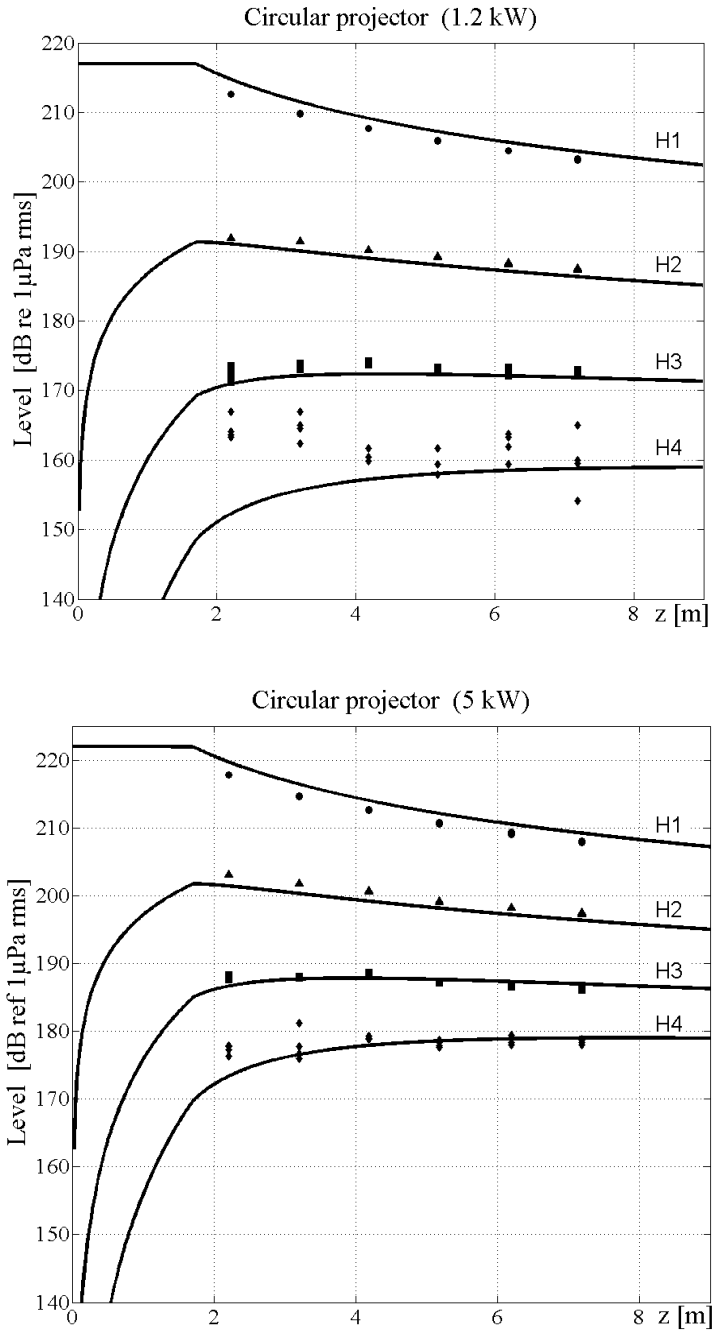

Figure 3. Harmonics level versus distance – Circular projector
(Nominal electric power P_e: top 1.2 kW, bottom 5 kW).
Numerical model (solid lines) and measurements (markers).

On the other hand, there is a systematic mismatch in the comparison performed with the rectangular source (Figure 4). The measured levels of harmonics are larger that expected, and the dynamic between the harmonics is tighter than with the modeled values.

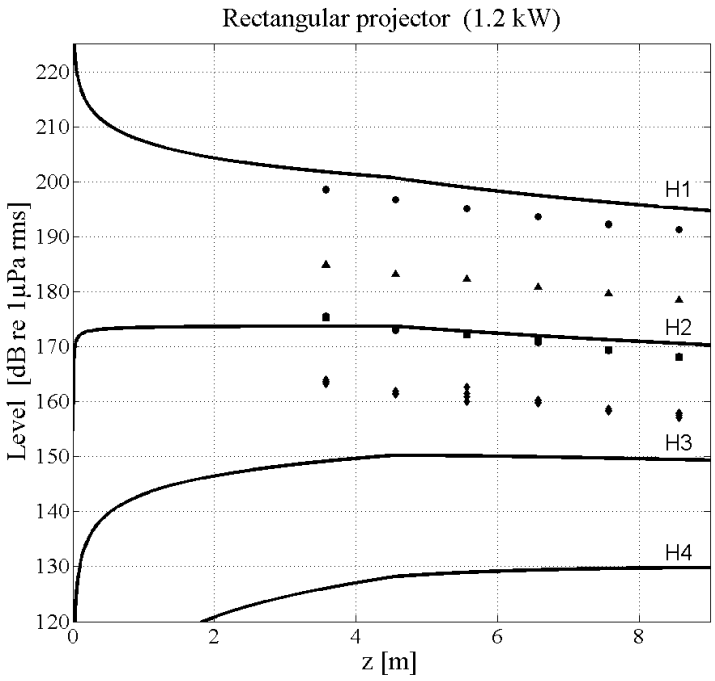

Figure 4. Harmonics level versus distance – Rectangular projector (P_e = 1.2 kW). Numerical model (solid lines) and measurements (markers).

A possible explanation is that the modeled field is not correct with this geometry. Most of the non linear interactions take place in the vicinity of the active face. The theoretical distance of the transition between plane and cylindrical propagations is the same order of magnitude as the wavelength (1.7 cm in Table I), hence meaningless. In the perpendicular plane, the classical modeling of the aperture linear radiation shows that there is a concentration of energy in the axial area just before the transition between the cylindrical and the spherical spreading regimes (Figure 5). This natural self focusing effect is not taken into account, although is can be suspected that it has a strong incidence in the building of the harmonics. An attempt has been made to alter the parameters of the model by imposing a smaller cross section of the transmitter, still keeping the same source power. Figure 6 shows that this change slightly increases the theoretical harmonic levels. However, the comparison with the measured levels is still not satisfactory.

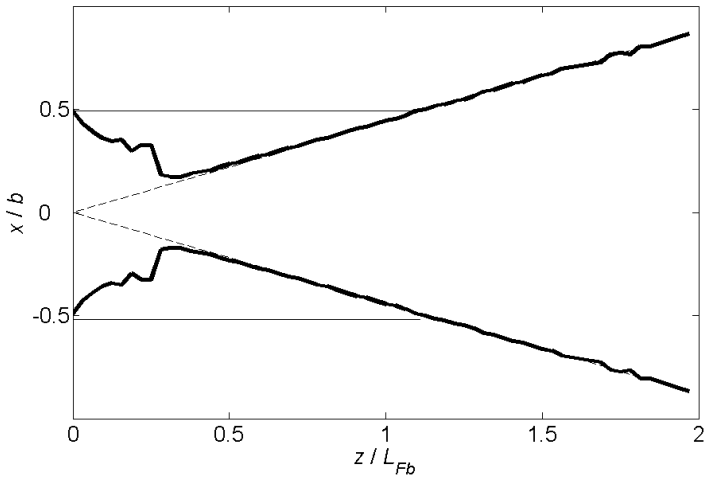

Figure 5. Phenomena of auto-focalisation in the near field.
Linear simulation for the rectangular aperture, in the most directive plane.
Solid line: -3dB contour line referenced to the on-axis level at the same *z* value.

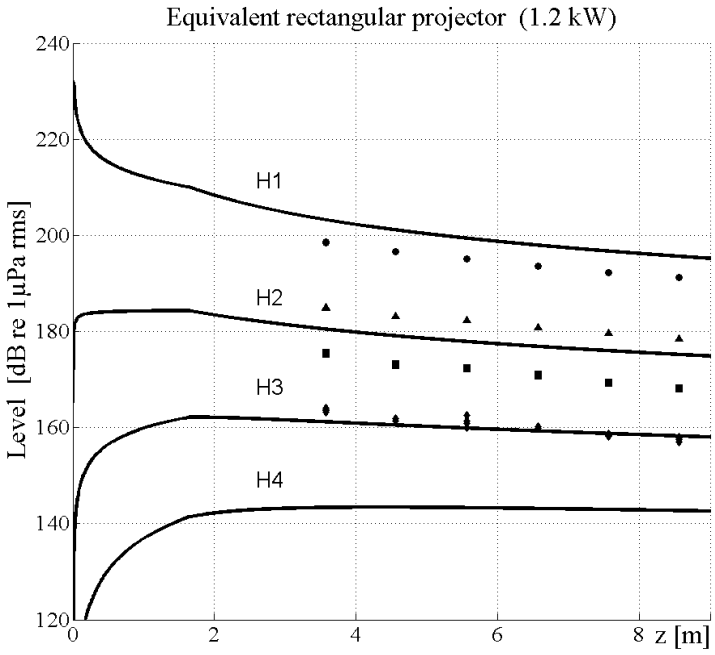

Figure 6. Harmonics level versus distance – Virtual source (1.2 kW).
Numerical model (solid lines) and measurements (markers).

The presented comparison shows clearly that the simple pseudo-1D model gives accurate orders of magnitudes for the on-axis levels of the harmonic fields generated by directive antennas. On the contrary, the model is not appropriate to handle large apertures: a more sophisticated description is called for.

The good news is that the absolute acoustic levels obtained with both antennas are quite large. The source levels of the first four harmonics range from 190 dB to 225 dB re 1µPa @ 1m for the disk. Although the transmitter sensitivity of the rectangular transducer is very penalized by its large aperture along one principal plane, the source levels are still in the range 175 dB to 210 dB re 1µPa @ 1m.

4.2. Beam patterns

Besides the achievable on-axis levels, the other issue that must be addressed with respect to the feasibility of the multi-harmonic transmitter is the characteristics of the beam patterns. Preliminary directivity measurements are displayed in Figures 7-8. The corresponding characteristic apertures are reported in Table III. These measurements are performed in a plane that is perpendicular to the z-axis (z = 6 m), i.e., not at a constant range. As expected, the higher is the harmonic, the narrower is the aperture. However, the beamwidth does not depend linearly on the frequency. The pseudo-1D model presented previously cannot estimate directivity diagrams. This problem calls for further experimental investigations, and comparisons with appropriate simulation tools.

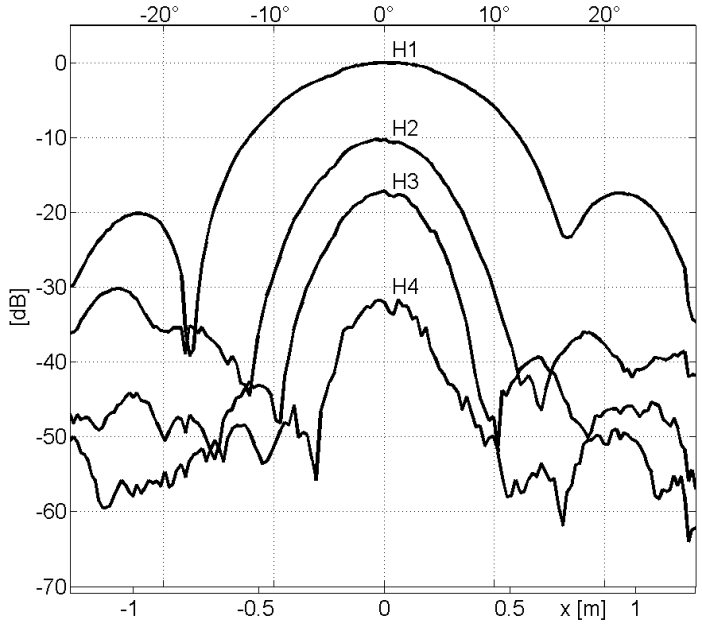

Figure 7. Directivity of the first harmonics – Circular projector (z = 6.3 m, P_e = 5 kW). Note that the circular symmetry is altered because the PZT elements are located along a spiral pattern.

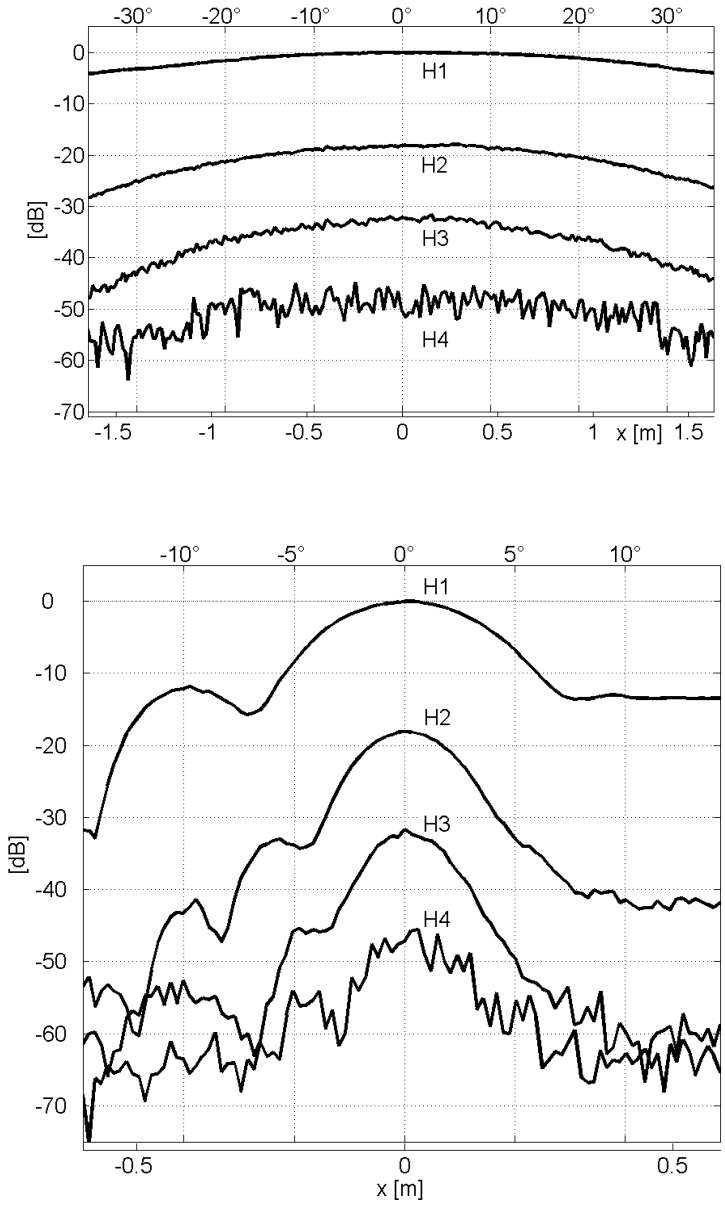

Figure 8. Directivity of the first harmonics with the rectangular projector (z = 4.8 m, P_e = 1.2 kW). Top: X-axis (the width of the tank is not large enough to measure the entire beam pattern). Bottom: Y-axis.

Table III. Beam width for both sources (z = 6 m).

	Circular projector	Rectangular projector	
		x-axis	y-axis
H1	5.6°	30°	3.1°
H2	3.6°	19°	1.9°
H3	2.7°	12°	1.4°
H4	2.3°	--	--

5. Conclusion

The goal of this work was to obtain a first evaluation about the feasibility of the multi-harmonic concept in the underwater domain. First experimental results show that quite large acoustic levels can be obtained. However, a considerable effort should be made to build a numerical model, e.g., based on [15][18][29], that allows to evaluate and to foresee the performance of antenna whose beam pattern is suitable for surveying tasks, i.e., with a large aperture in one plane. A prospective embodiment is a sidescan multifrequency sonar system. In the perspective of sediment characterization, the possibility to develop a multi-frequency source at a lower fundamental frequency (typically 40 kHz) is studied. This would enable to probe the seafloor by giving a significant contribution from volume scattering, whereas higher harmonics provide information about the roughness at different scales.

Acknowledgment

The work has been and is supported by IFREMER.

1 P. Cervenka and J. Marchal, Imaging with a new multi-look front-scan sonar system, Acta Acustica / Acustica **90** 1, 38-48, 2004..

2 X. Lurton, J-C. Legac, The CALIMERO project: scientific objectives and first at-sea results, Proc. SeaTechWeek 2004, In-situ seabed characterization, Brest 21-22 october 2004. http://www.ifremer.fr/dtmsi/colloques/seatech04/xlurton/A6_Scientific_applications_2/Lurton_LeGac.pdf (last seen 16 june 2010)

3 F. Parthiot, E. de Nanteuil, F. Merlin, B. Zerr, Y.Guedes, X. Lurton, J.-M. Augustin, P. Cervenka, J.Marchal, J.P. Sessarego, R. K.Hansen, Sonar detection and monitoring of sunken heavy fuel oil on the seafloor, NOSCA, Proceedings Interspill 2004 conference, 14-17 juin 2004, Trondheim. http://www.interspill.com/PDFs/UK/2004/465_PARTHIOT.pdf (last seen 16 june 2010)

4 T.G. Muir, Nonlinear effects in acoustic imaging, Acoust. Imag., **9**, 93, 1980.

5 L. Bjørnø, P.A. Lewin, Nonlinear focusing effects in ultrasonic imaging, Ultrasonic Symp. IEEE, 659, 1982.

6 B. Ward, A.C. Backer, V.F. Humphrey, Nonlinear propagation applied to the improvement of resolution in diagnostic medical ultrasound, J. Acoust. Soc. Am. **101**, 143, 1997.

7 M. Claudon, F. Tranquart, D.H. Evans, F. Lefèvre, J.M. Correas, Advances in ultrasound, Eur Radiol 12:7–18, 2002.

8 J.E. Browne, A.J. Watson, N.M. Gibson, N.J. Dudley, A.T. Elliott, Objective measurements of image quality, Ultrasound in Med. & Biol. **30**, 229-237, 2004.

9 J. Marchal, P. Cervenka, Modeling of the parametric transmission with the spatial Fourier formalism. Optimization of a parametric antenna, Acta Acustica / Acustica **90**, 49-61 (2004).

10 J.A. Shooter, T.G. Muir, D.T. Blackstock, Acoustics saturation of spherical waves in water, J. Acoust. Soc. Am. **55**, 54, 1974.

11 B.K. Novikov, O.V. Rudenko, V.I. Timoshenko (1987), Nonlinear underwater acoustics, Translation Series, American Institute of Physics (New York)

12 D.T. Blackstock, Generalized Burgers equation for plane waves, J. Acoust. Soc. Am. **77**, 2050, 1985.

13 S.I. Aanonsen, T. Barkve, J. Naze Tjőtta, S. Tjőtta, Distortion and harmonic generation in the nearfield of a finite amplitude sound beam, J. Acoust. Soc. Am. **75**, 749–768, 1984.

14 Y-S. Lee, M.F. Hamilton, Time-domain modeling of pulsed finite-amplitude sound beams, J. Acoust. Soc. Am. **97**, 906, 1995.

15 R.O. Cleveland, M.F. Hamilton, D.T. Blackstock, Time-domain modeling of finite-amplitude sound in relaxing fluids, J. Acoust. Soc. Am. **99**, 3312, 1996.

16 X. Yang, R.O. Cleveland, Time domain simulation of nonlinear acoustics beams generated by rectangular pistons with application to harmonic imaging, J. Acoust. Soc. Am. **117**, 113, 2005.

17 J. Tavakkoli, D. Cathignol, R. Souchon, O.A. Sapozhnikov, Modeling of pulsed finite-amplitude focused sound beams in time domain", J. Acoust. Soc. Am. **104**, 2061-2072, 1998.

18 M. Rénier, F. Dagrau, R. Marchiano, F. Coulouvrat, 'HOWARD' : un modèle pour la propagation d'ondes de choc acoustiques en milieu hétérogène, au delà de l'approximation parabolique, 10ème Congrès Français d'Acoustique, Lyon 12-16 avril 2010.

19 M.F. Hamilton, D.T. Blackstock, Nonlinear acoustics, Chapter 3, Academic Press Inc., 2002.

20 V.P. Kuznetsov, Equations of nonlinear acoustics, Sov. Phys. Acoust. **16**(4), 467-470, 1970

21 A.D. Pierce, Acoustics: an introduction to its physical principles and applications, ch. 11, Acoustical Society of America, New-York, 1989.

22 R.E. Francois, G.R. Garrison, Sound absorption based on ocean measurements: Part II: Boric acid contribution and equation for total absorption, J. Acoust. Soc. Am. **72**, 1879, 1982.

23 M. B. Moffett, R. H. Mellen, and W. L. Konrad, "Parametric acoustic sources of rectangular aperture" J. Acoust. Soc. Am. **63**, 1326-1331 (1978).

24 W.F. Ames, Numerical methods for partial differential equations, Boston, Academic Press, 1992.

25 G. Strang, On the construction and comparison of difference schemes, SIAM J. Numer. Anal **5**(3), 506-517, 1968.

26 M.A. Averkiou, M.F. Hamilton, 'Nonlinear distortion of short pulses radiated by plane and focused circular pistons, J. Acoust. Soc. Am. **102**, 2539–2548, 1997.

27 N. S. Bakhvalov et al, Nonlinear Theory of Sound Beams, American Institute of Physics, New York, 1987.

28 F.M. Pestorius, T.D. Blackstock, Propagation of finite-amplitude noise, in Finite –Amplitude wave effects in fluids, ed. Bjørnø (IPC Science and Technology Press), 24-29, 1974.

29 R. Marchiano, F. Coulouvrat, L. Ganjehi, J-L Thomas, Numerical investigation of the properties of nonlinear acoustical vortices through weakly heterogeneous media, Physical Review E **77**, 016605-1-11 (2008).

30 J.R. Lovett, Merged seawater sound-speed equations, J. Acoust. Soc. Am. **63**, 1713, 1978.